View metadata, citation and similar papers at core.ac.uk
brought to you by CORE
provided by CiteSeerX

Materials Transactions, Vol. 49, No. 12 (2008) pp. 2844 to 2849
©2008 The Japan Institute of Metals

Weldability of Nickel-Free Austenitic Stainless Steel Thin Sheet by Small-Scale Resistance Spot Welding

Shinji Fukumoto[1], Taiju Matsuo[1,*], Daisuke Kuroda[2] and Atsushi Yamamoto[1]

[1]*Graduate School of Engineering, University of Hyogo, Himeji 671-2201, Japan*
[2]*Suzuka National College of Technology, Suzuka 510-0294, Japan*

The feasibility and microstructural development of high-nitrogen-containing nickel-free austenitic stainless steel by small-scale resistance spot welding were studied. Almost fully austenitic cellular microstructure was developed in weld nuggets because the cooling rate of approximately 10^5 Ks^{-1} was much faster than that in conventional fusion welding processes. Only a small amount of delta ferrite was formed at the gamma grain boundary in the weld, and chromium nitride precipitation was observed both in the gamma grains and at the grain boundary. No significant defects and sensitization were observed in the weld nugget and in the heat affected zone, respectively, and an adequate joint strength was obtained. [doi:10.2320/matertrans.MRA2008285]

(Received August 19, 2008; Accepted September 2, 2008; Published October 16, 2008)

Keywords: *small-scale resistance spot welding, nickel-free austenitic stainless steel, microstructure, cooling rate*

1. Introduction

Austenitic stainless steels such as type 316L are widely used in medical devices because of their superior corrosion resistance and mechanical properties. However, they normally contain a large amount of nickel; nickel is well known to be toxic to humans. Therefore, Cr-Ni austenitic stainless steels[1–3] have been modified to develop high-nitrogen-containing nickel-free stainless steels. Nitrogen is known to enhance the austenite stability with respect to deformation-induced martensite formation,[2–4] and it also improves the pitting corrosion resistance of the above-mentioned stainless steels. On the other hand, since nitrogen results in poor workability of stainless steels, their use would not be preferred in the manufacture of small and complex medical devices. Therefore, welding techniques, especially those applicable at the small or micro scales, are required to popularize the usage of nickel-free stainless steels in the medical field.

Micro- or small-scale resistance spot welding (SSRSW) processes have been developed on the basis of several microjoining processes (such as resistance spot, parallel gap, series, cross-wire, and seam welding) in which a microjoint (thickness of sheet metal: less than 0.2–0.5 mm) is formed between two sheets or wires by resistance heating caused by the passage of an electric current.[5–8] These processes are commonly used for applications in electronic and medical devices; however, despite their increasing number of applications, limited research has been conducted in this area. In comparison, extensive studies have been carried out on 'large-scale' resistance spot welding (LSRSW) of a sheet metal thicker than 0.5 mm.[9,10] There are several differences between SSRSW and LSRSW. Simply downsizing from LSRSW to SSRSW may lead to various drawbacks such as electrode sticking, weld metal expulsion, and non-repeatable welding.[6,11,12] Furthermore, since metals to be welded by SSRSW are mostly nonferrous,[13–15] there has been limited research on SSRSW of steels.[16]

In general, the joints characteristics in fully austenitic stainless steels, such as mechanical properties, corrosion resistance, and magnetic properties, depend on the microstructure of the weld. For example, it is a well-known fact that a small amount delta ferrite in the weld prevents the hot cracking of joints.[17,18] On the other hand, a small amount of ferrite may also affect the magnetic resonance image (MRI) scan. Therefore, evaluating the microstructural development of welds is important from the point of view of the manufacture of medical devices.

In the present study, the microstructural development and weldability of high-nitrogen-containing nickel-free austenitic stainless steel by SSRSW were investigated.

2. Experimental Procedures

In this study, a 200-μm-thick nickel-free austenitic stainless steel sheet that was fabricated by nitrogen absorption treatment was used; its chemical composition is listed in Table 1. The details of the nitrogen absorption treatment are described elsewhere.[3] Tensile strength of the alloy is 1170 MPa. SSRSW was carried out in an air atmosphere. The welding system consisted of a Miyachi Technos MH-D20A weld head (servo activated) and a Miyachi Technos MDB-2000 direct-current (DC) power supply. Flat-ended, round, class II (Cu-Cr) electrodes of 3-mm diameter were used. The welding force and weld time were 58.8 N and 9.0 ms, respectively. The welding current was varied from 400 to 2000 A with no current ramp-up or ramp-down times. Prior to welding, the sample surfaces were polished with emery papers and cleaned with acetone. Moreover, gas tungsten arc welding (GTAW) was carried out on some samples for comparison with SSRSW. The cross sections of the welds were examined using optical microscopy and scanning electron microscopy (SEM) (JSM-6360) together with electron backscattering diffraction patterns (EBSPs) (TSL MSC-2200). The surfaces of these samples used for EBSP analysis were finished using a colloidal silica suspension. Metallographic samples for optical microscopy were prepared by electrolytic etching (4 V, 20 s) using a solution of

*Graduate Student, University of Hyogo

Table 1 Chemical composition of nickel free stainless steel. (mass%)

C	Mn	P	S	Ni	Cr	Mo	O	N	Fe
0.005	<0.01	<0.01	<0.001	<0.01	23.4	1.95	0.03	1.24	Bal.

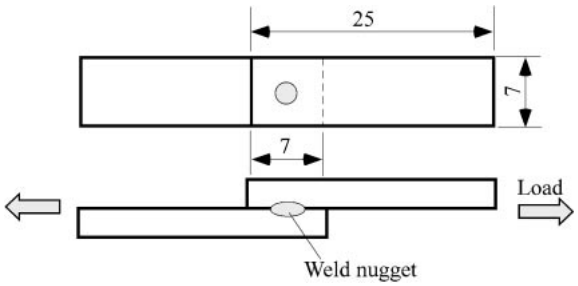

Fig. 1 Schematic of test coupon and tensile shear test. (unit: mm)

10% oxalic acid. The microstructure of the weld nugget was observed by transmission electron microscopy (TEM, JEM-200CX). Nitrogen concentration in the weld nugget was measured by electron probe micro-analysis (EPMA). A micro-area X-ray diffraction (XRD) measurement was carried out at 40 kV and 150 mA to identify phases in weld nuggets. The diameter of collimator is 100 μm. A synchrotron radiation (SR) diffraction measurement (SPring-8, BL24XU) was also carried out at a beam energy of 10 keV to identify different phases in weld nuggets. Lap welded joints were made using test coupons cut to approximately 25 mm length and 7 mm width. Joint quality was evaluated using a tensile shear test (Fig. 1) that was performed at a cross-head speed of 0.02 mm s^{-1}. Nugget diameter was estimated by measuring the diameter of weld area on the fractured surfaces after the tensile shear test.

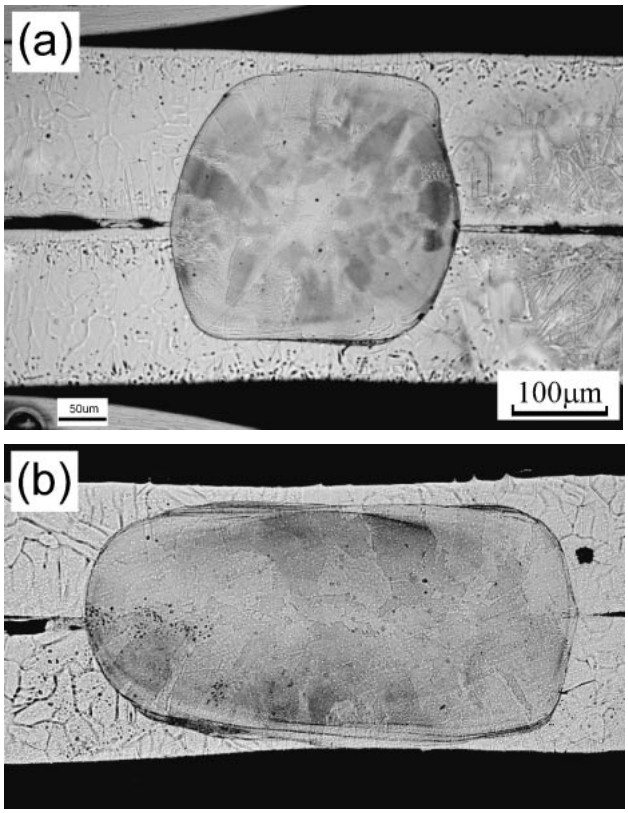

Fig. 2 Cross sections of weld nuggets, (a) 1000 A and (b) 1400 A.

3. Results

3.1 Microstructures

Figure 2 shows the cross sections of joints produced under the welding currents of 1000 and 1400 A. Weld nugget was obtained when the welding current was over 500 A, and the nugget size increased with the welding current. No defects such as hot cracks and worm holes were observed in the weld nuggets when the welding current was less than 1400 A. The weld metal expulsion and/or tiny porosity were observed in some cases. When the welding current was over 1600 A, serious surface flash occurred, resulting in the electrode/sheet sticking and/or surface indentation. Figure 3 shows the microstructure of weld nugget and its vicinity. The substructure of weld nugget exhibited a cellular structure and an almost fully austenitic microstructure. There was no delta ferrite in the weld nuggets, as observed by optical microscopy. Base metal grains at the fusion line acted as the substrate for nucleation, resulting in epitaxial growth at the fusion boundary. The authors reported that heat affected zone (HAZ) with recrystallization was formed surrounding the weld nugget in the case of SSRSW of the conventional cold-rolled austenitic stainless steel sheets that originally shows the microstructure with elongated grains.[19] In the present study, since the base alloy is manufactured by the nitrogen absorption method at the high temperature, the microstructure of the base alloy has equiaxed grains by nature. Therefore no recrystallization was observed in the HAZ. However, the partially melted zone was observed at the grain boundary in HAZ due to low melting point constituents segregated at the grain boundaries.[20] It is well known that not only hot cracking but also sensitization in HAZ are important problems in welding austenitic stainless steels. Not a ditch but a step structure was observed in the HAZ under any welding conditions, which means that sensitization was negligible in the present study.

In general, the delta ferrite content in the stainless steel weld is estimated by the following methods, namely, a ferrite scope, which is one of the methods used for magnetic measurements, XRD analysis, or microstructural observation.[21] When the weld area is considerably small, such as that in small-scale welding, magnetic measurements cannot be carried out to detect the presence of ferrite. In this study, optical microscopy indicated a fully austenitic structure in the weld nugget. However, David *et al.* reported transmission electron microscopy (TEM) revealed the presence of an occasional grain of ferrite in the structures of laser beam welded type 308 stainless steel characterized as fully austenitic by optical microscopy.[22] Robino *et al.* reported that the backscattered electron Kikuchi pattern in SEM is

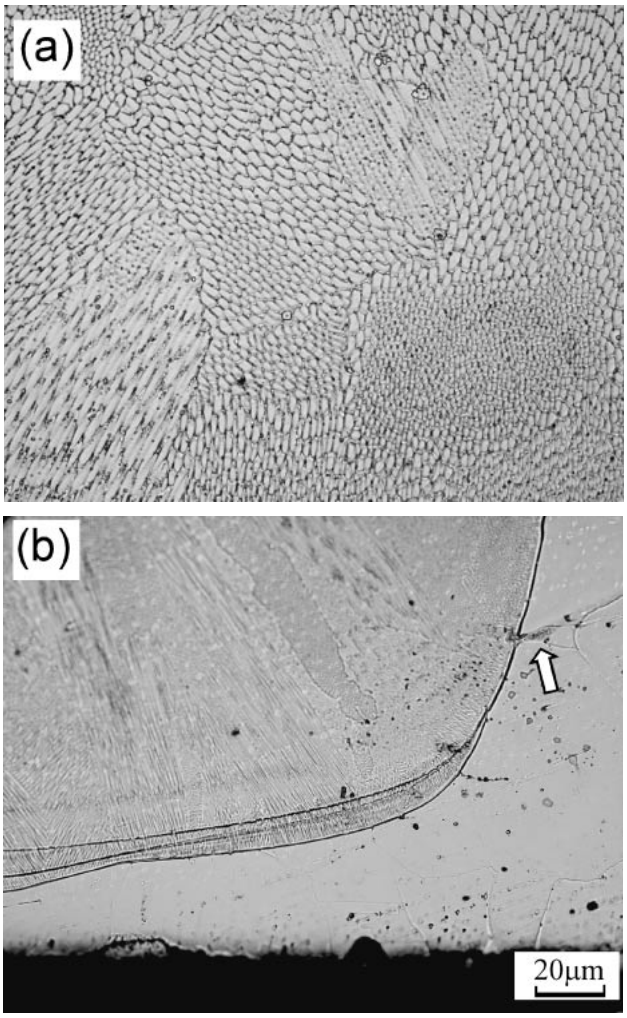

Fig. 3 Microstructure of weld nugget: (a) center and (b) fusion boundary. The arrow shows the partially melted zone in the HAZ.

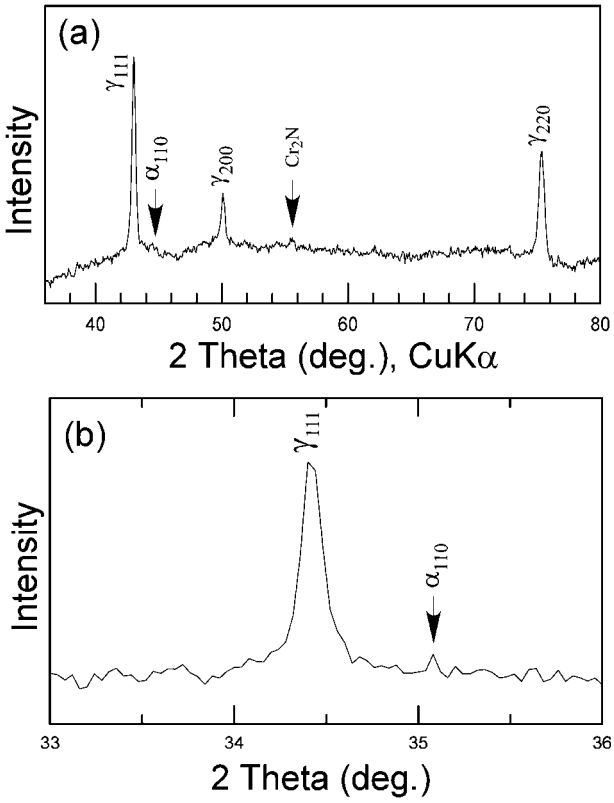

Fig. 4 X-ray (a) and synchrotron radiation (b) diffraction patterns of weld nugget.

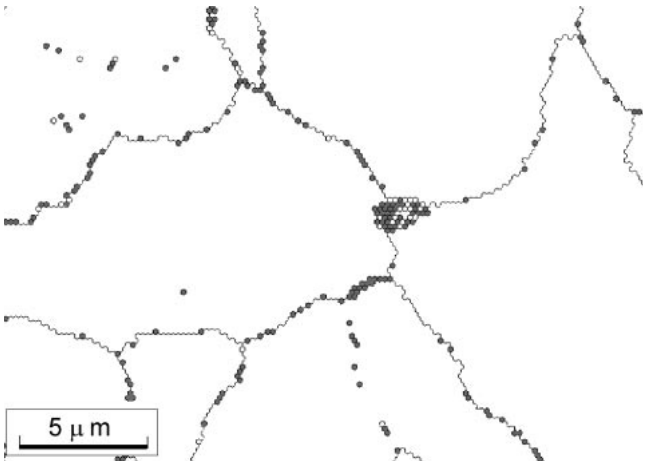

Fig. 5 EBSP mapping of ferrite and austenite in weld nugget made with the welding current of 1400 A. Gray region shows ferrite.

useful for identifying ferrite and austenite in the weld of stainless steels.[23] Authors also reported SEM-EBSP analysis is useful for detecting the small amount of delta-ferrite present in a small region such as a small weld nugget.[19] Then in the present study, micro-area XRD and SR analysis and TEM observation were carried out to investigate micro-structural development during SSRSW. Figure 4 shows the micro-area XRD and synchrotron radiation diffraction patterns of the weld nugget made with the welding current of 1400 A. Almost fully austenite phase was identified by these analyses as well as optical microscopy. In addition, a small trace of ferrite and chromium nitride was identified, too. The EBSP mapping for ferrite in the weld nugget developed by SSRSW is shown in Fig. 5. Only a small trace of ferrite was found at the austenite grain boundary. Figure 6 shows the TEM bright field image of the weld nugget and the selected area diffraction pattern of Cr_2N precipitates. The Cr_2N precipitates were observed in the gamma grains as well as at the grain boundary. Although a small amount of Cr_2N precipitates were formed in the weld nugget, the nitrogen concentration did not change significantly as detected by an EPMA. Nitrogen concentration was 1.4 mass% in the base alloy as detected by EPMA. On the other hand, nitrogen concentration in the weld was in the range of 1.2 to 1.4 mass%. Consequently, the alloy solidified with austenite as the primary phase, and only a small amount of ferrite and chromium nitride were precipitated.

3.2 Joint strength

Figure 7 shows the weld nugget diameter and shear force of the joints as a function of welding current. No weld was obtained when the welding current was less than 400 A. It is noted that the welding current threshold to make a weld depends on the other welding conditions, especially the welding force. In general, the welding current threshold increases with an increase of welding force due to a decrease

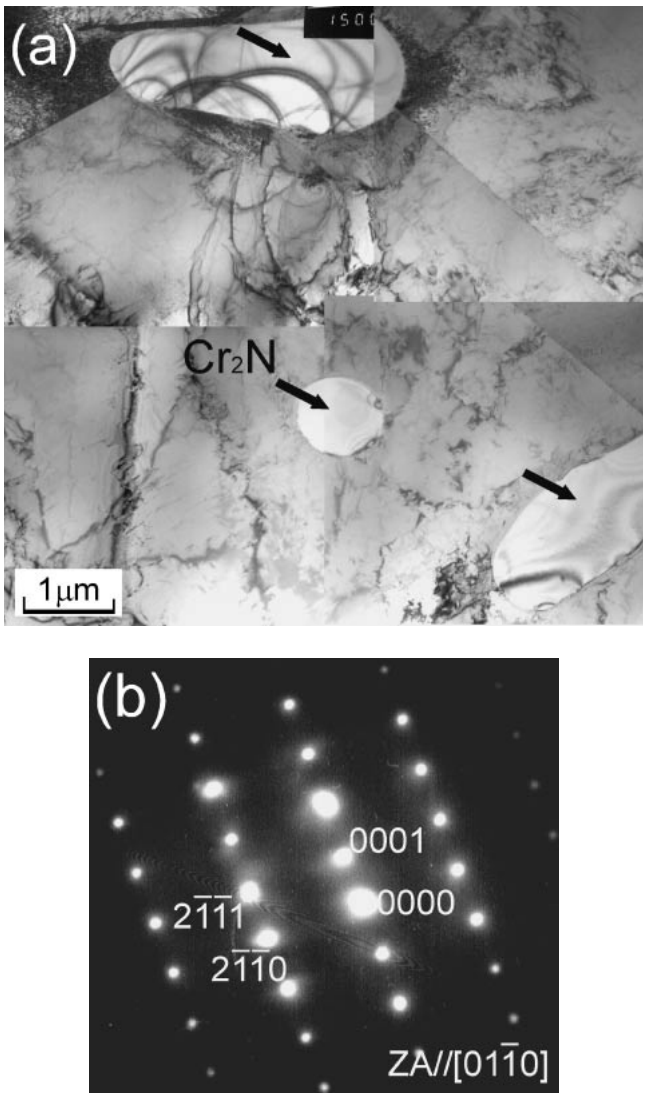

Fig. 6 TEM images of weld nugget made with 1400 A of welding current. (a) Bright field image and (b) Selected area diffraction pattern of Cr_2N precipitates. They were located in gamma grains as well as at the grain boundary.

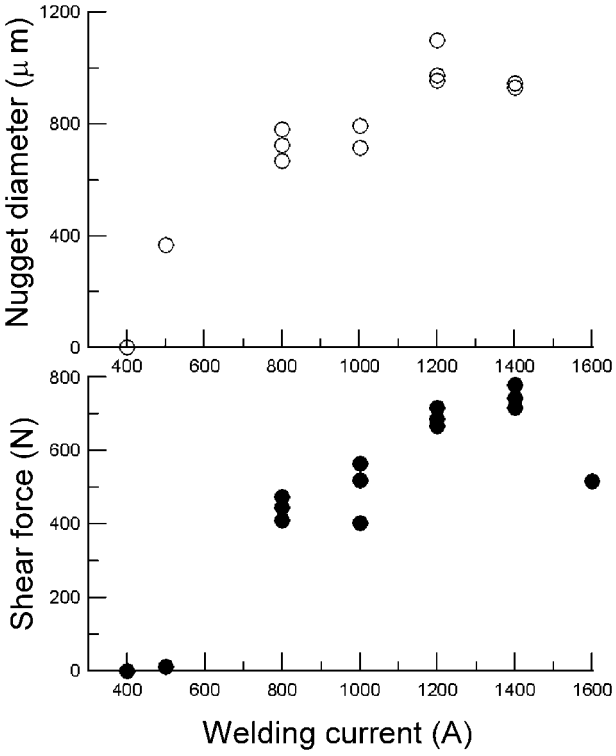

Fig. 7 Effect of welding current on nugget diameter (a), and shear force of joints (b).

of contact resistance at the faying interface.[19] As shown in Fig. 2, the weld nugget grew as the welding current increased, resulting in an increase in shear force. The joints exhibited good mechanical properties, except under the condition of a severe surface flash or electrode-sheet sticking such as the condition of 1600 A. The tensile shear strength of the sound joints that is calculated from shear force and nugget diameter was approximately 650 MPa, which is almost equal to half the tensile strength of the base alloy.

4. Discussion

The Schaeffler diagram is often used to predict microstructures of weld metal in the case of conventional stainless steels. Schaeffler first proposed the quantitative relation between the composition and ferrite content of the weld metal. Many researchers including DeLong refined Schaeffler's diagram to include nitrogen, a strong austenite former as new stainless steels were developed. Although the constitutional diagram for the present alloy has not investigated in detail, some modified diagrams considering nitrogen and manganese were used to predict the microstructural development of the present alloy. Figure 8 shows some modified diagrams[2,24,25] with the plot for the present alloy. The alloy could solidify as a primary austenite, and the amount of ferrite is estimated at most 5% according to those diagrams. In fact, the amount of delta-ferrite in the weld nugget was minimal.

According to the Schaeffler diagrams or the predictions using similar Cr and Ni equivalents, the amount of ferrite present in the weld depends only on the weld composition, and it is independent of the welding conditions. For most welding conditions, this appears to be true. It is noted that the prediction of the weld metal ferrite content based on the constitutional diagrams can be inaccurate when the cooling rate is high, especially in laser and electron beam welding.[26] For example, Nakao *et al.* have reported that the fast cooing rate in laser beam welding reduced (gamma + delta) the two-phase field in the original Schaeffler diagram, and the solidification mode transformed from primary austenite to fully austenite or from primary ferrite to massive solidification.[27,28] Elmer *et al.* reported that in general low Cr-Ni ratio alloys solidify with austenite as the primary phase, and their ferrite content decreases with increasing cooling rate.[29] Authors also reported that SSRSW of stainless steels exhibits a fast cooling rate that is almost equal to that of laser welding, and the amount of delta ferrite was lesser than that estimated by the Schaeffler diagrams.[19] In Ref. 28), the relation between the cell size (D) and the cooling rate (C_R) is shown in terms of the following equation.

$$D = 58\{C_R\}^{-0.32} \quad (1)$$

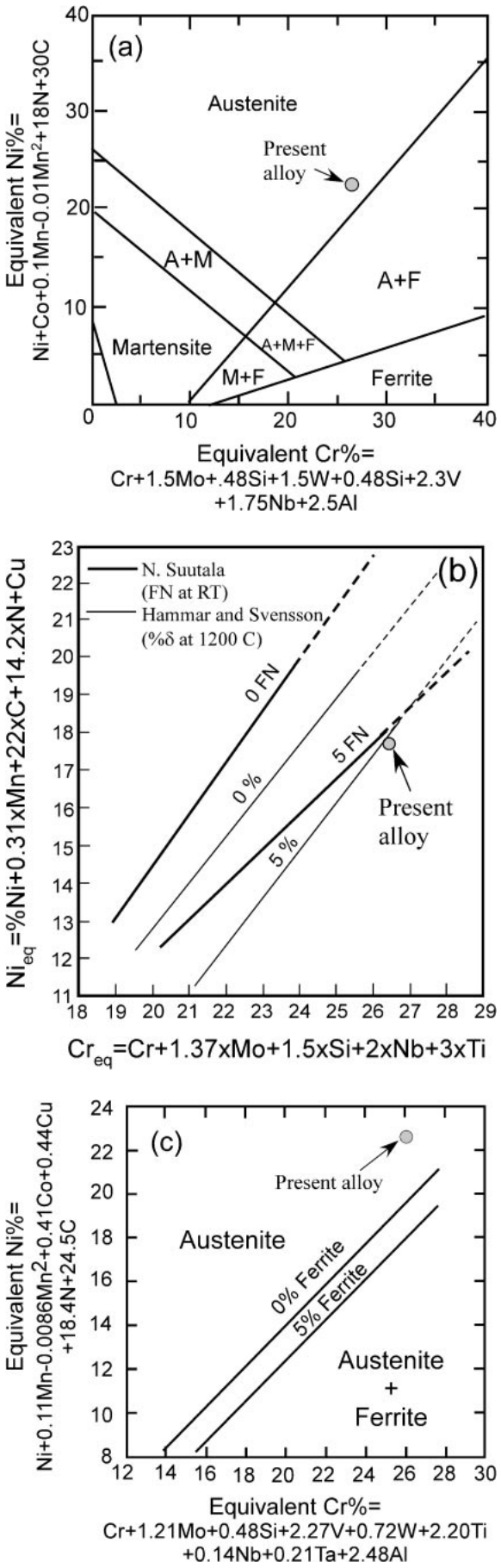

Fig. 8 Modified Schaeffler's diagrams by (a) Uggowitzer *et al.*,[2] (b) Suutala *et al.*[24] and (c) Hull[25] with the plot of present alloy.

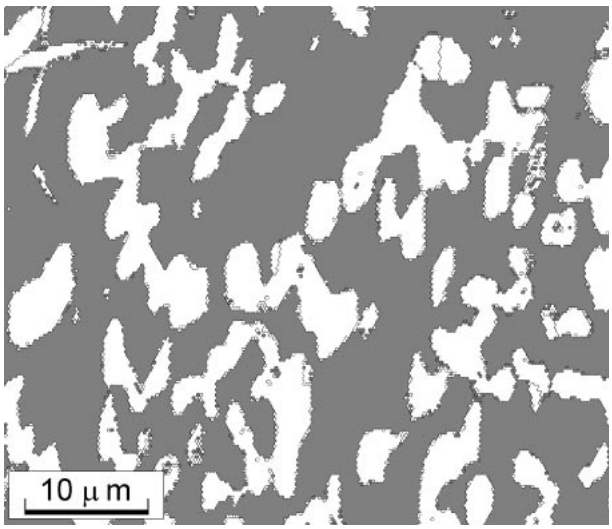

Fig. 9 EBSP mapping of gamma and delta phases in the weld developed by GTA welding. White and gray regions show gamma and delta phases, respectively.

The cell size in the weld nugget was varied from 0.8 to 1.7 μm. In the present study, cooling rate was calculated to be approximately 6.2×10^4 to 6.5×10^5 K s^{-1} from eq. (1); this rate is considerably faster than that in conventional fusion welding processes such as GTAW.

In order to compare conventional fusion welding with the process used in our study, we carried out the conventional fusion welding such as GTAW that exhibited a cooling rate of approximately 10^3 K s^{-1}. Approximately 60% delta ferrite that is larger than the value predicted from the Schaeffler diagram was formed in the weld (Fig. 9), and the concentration of nitrogen in the weld was decreased to approximately 0.5 mass%. Denitrogenation occurred during GTAW since the weld pool is exposed to the atmosphere. Similar results, that are nitrogen loss in high nitrogen stainless steel during GTAW, have been reported by Brooks.[30] The reduction in the austenite former element due to denitrogenation results in an increase in the amount of delta ferrite. On the other hand, the weld nugget is formed in a closed space due to the nature of the resistance spot welding process. Sawairi *et al.* also reported that nitrogen loss was not detected in the weld nugget of high nitrogen 18Cr-10Mn stainless steel by LSRSW.[31] Thus, nitrogen is retained in the weld nugget in the RSW.

Chromium nitride precipitation and porosity should also be noted in the welding of high-nitrogen containing nickel free stainless steel. As described above, fast cooling rate as well as fast heating rate due to high energy density heat source is the most significant characteristic for RSW, especially in small-scale because faster cooling rate is expected in thinner sheet in RSW.[32] Woo *et al.* pointed out Cr_2N was formed in HAZ, ant its amount increases with decreasing cooling rate.[33] The fast cooing rate makes Cr_2N precipitate minimal in the case of SSRSW.

Effect of weld parameters on the formation of porosity has not been clarified in the present study. Sawairi *et al.* reported the formation of porosity seemed to have relate to the weld metal expulsion.[31] Further systematic studies are needed to investigate the mechanism of porosity formation.

5. Conclusions

The high-nitrogen-containing nickel-free stainless steel developed for the medical implants was welded by SSRSW. The weldability and microstructural development were evaluated. SSRSW could be a suitable process for welding the high-nitrogen-containing nickel-free austenitic stainless steel used in medical devices. The results and conclusions are summarized as follows.

(1) Optical microscopy revealed that almost fully austenitic with cellular structure was produced by SSRSW. Hot cracking was not observed despite little delta ferrite. Sensitization was not observed in the HAZ welded under any welding currents.
(2) SEM-EBSP, micro-area XRD and SR analyses detected that only a small trace of delta ferrite was formed at the austenite grain boundary. Chromium nitride was also formed at the grain boundary and in the austenite grains. However, significant loss in nitrogen was not detected in the weld nugget.
(3) The cooling rate of SSRSW is estimated at approximately 6.2×10^4 to $6.5 \times 10^5\,\mathrm{K\,s^{-1}}$, resulting in reducing delta ferrite.
(4) Sound joints were obtained in the rage of welding current from 500 to 1400 A. The joint quality is almost equal to the base alloy.

Acknowledgements

This research was partially supported by the Ministry of Education, Culture, Sports, Science and Technology, Japan, Grant-in-Aid for Scientific Research (C) (No. 16560638). Experimental assistance by Kana Fujiwara, Osaka Prefecture University, in this study is greatly appreciated.

REFERENCES

1) J. Menzel, W. Kirschner and G. Stein: ISIJ Int. **36** (1996) 893–900.
2) P. J. Uggowitzer, R. Magdowski and M. O. Speidel: ISIJ Int. **36** (1996) 901–908.
3) D. Kuroda, T. Hanawa, T. Hibaru, S. Kuroda, M. Kobayashi and T. Kobayashi: Mater. Trans. **44** (2003) 414–420.
4) Y. Ikegami and R. Nemoto: ISIJ Int. **36** (1996) 855–861.
5) E. F. Koshinz: Weld. Design Fabrication **45** (1972) 76–79.
6) D. Steinmeier: Weld. J. **77** (1998) 39–47.
7) S. Fukumoto and Y. Zhou: Metall. Mater. Trans. A **35A** (2004) 3165–3176.
8) S. Fukumoto, Zheng Chen and Y. Zhou: Metall. Mater. Trans. A **36A** (2005) 2717–2724.
9) J. G. Kaiser, G. J. Dunn and T. W. Eagar: Weld. Res. Suppl. **61** (1982) 167s–174s.
10) E. P. Patrick, J. R. Auhl and T. S. Sun: SAE Technical Paper, 840291, Int. Cong. & Expo., Detroit, Michigan, (1984).
11) B. H. Chang, M. V. Li and Y. Zhou: Sci. Technol. Weld. Join. **6** (2001) 273–280.
12) S. J. Dong, G. P. Kelkar and Y. Zhou: IEEE Trans. Electron. Packag. Manuf. **25** (2002) 355–361.
13) W. Tan, Y. Zhou and H. W. Kerr: Metall. Mater. Trans. A **33A** (2002) 2667–2676.
14) Y. Zhou, P. Gorman, W. Tan and K. J. Ely: J. Electron. Mater. **29** (2000) 1090–1099.
15) W. Tan, Y. Zhou, H. W. Kerr and S. Lawson: J. Phys. D **37** (2004) 1998–2008.
16) K. J. Ely and Y. Zhou: Sci. Technol. Weld. Join. **6** (2001) 63–72.
17) J. C. Villaruerte and H. W. Kerr: Key Eng. Mater. **69&70** (1992) 129–148.
18) J. A. Brooks, A. W. Thompson and J. C. Williams: Weld. Res. Suppl. **63** (1984) 71s–83s.
19) S. Fukumoto, K. Fujiwara, S. Toji and A. Yamamoto: Mater. Sci. Eng. A **492** (2008) 243–249.
20) K. Sindo: *Welding Metallurgy 2nd edn*, (Hoboken, New Jersey, John Wiley & Sons, Inc., 2003) pp. 303–320.
21) W. T. DeLong: Weld. Res. Suppl. **53** (1974) 273s–286s.
22) S. A. David, J. M. Vitek and T. L. Hebble: Weld. Res. Suppl. October (1987) 289s–300s.
23) C. V. Robino, J. R. Michael and M. C. Maguire: Weld. Res. Suppl. November (1998) 446s–457s.
24) N. Suutala: Metall. Trans. A **13A** (1982) 2121–2130.
25) F. C. Hull: Weld. Res. Suppl. May (1973) 193s–203s.
26) K. Sindo: *Welding Metallurgy 2nd edn*, (Hoboken, New Jersey, John Wiley & Sons, Inc., 2003) pp. 216–242.
27) Y. Nakao, K. Nishimoto and W.-P. Zhang: Quart. J. Jpn. Weld. Soc. **9** (1991) 111–116.
28) Y. Nakao, K. Nishimoto and W.-P. Zhang: Quart. J. Jpn. Weld. Soc. **7** (1989) 414–421.
29) J. W. Elmer, S. M. Allen and T. W. Eagar: Metall. Trans. **20A** (1989) 2117–2131.
30) J. A. Brooks: Weld. Res. Suppl. June (1975) 189s–195s.
31) M. Sawairi and R. Tanaka: J. Jpn. Weld. Soc. **39** (1970) 117–123.
32) J. E. Gould, S. P. Khurana and T. Li: Weld. J. May (2006) 111s–116s.
33) I. Woo, T. Horinouch and Y. Kikuchi: Trans. JWRI **30** (2001) 77–84.